BMC Biology

RESEARCH ARTICLE

Open Access

Pangolin scales as adaptations for innate immunity against pathogens

Xuechen Tian[1,2,3†], Li Chen[4†], Jinfeng Zhou[5], Enbo Wang[1], Mu Wang[6], Nicholas Jakubovics[7], Jing Li[6], Kunping Song[1], King Tong Lau[6], Klaus-Peter Koepfli[8,9], Siyuan Zhang[5], Geok Yuan Annie Tan[4], Yixin Yang[1,2,3,10] and Siew Woh Choo[1,2,3,10*]

Abstract

Background Pangolins are the only mammals that have overlapping scales covering most of their bodies, and they play a crucial role in the ecosystem, biological research, and human health and disease. Previous studies indicated pangolin scale might provide an important mechanical defense to themselves. The origin and exact functions of this unique trait remain a mystery. Using a multi-omics analysis approach, we report a novel functional explanation for how mammalian scales can provide host–pathogen defense.

Results Our data suggest that pangolin scales have a sophisticated structure that could potentially trap pathogens. We identified numerous proteins and metabolites exhibiting antimicrobial activity, which could suggest a role for scales in pathogen defense. Notably, we found evidence suggesting the presence of exosomes derived from diverse cellular origins, including mesenchymal stem cells, immune cells, and keratinocytes. This observation suggests a complex interplay where various cell types may contribute to the release of exosomes and antimicrobial compounds at the interface between scales and viable tissue. These findings indicate that pangolin scales may serve as a multifaceted defense system, potentially contributing to innate immunity. Comparisons with human nail and hair revealed pangolin-specific proteins that were enriched in functions relating to sensing, immune responses, neutrophil degranulation, and stress responses. We demonstrated the antimicrobial activity of key pangolin scale components on pathogenic bacteria by antimicrobial assays.

Conclusions This study identifies a potential role of pangolin scales and implicates scales, as possible determinants of pathogen defense due to their structure and contents. We indicate for the first time the presence of exosomes in pangolin scales and propose the new functions of scales and their mechanisms. This new mechanism could have implications for multiple fields, including providing interesting new research directions and important insights that can be useful for synthesizing and implementing new biomimetic antimicrobial approaches.

Keywords Pangolin, Mammalian scale, Antibacterial, Exosome, Host–pathogen defense, Innate immunity

†Xuechen Tian and Li Chen contributed equally to this work.

*Correspondence:
Siew Woh Choo
cwoh@wku.edu.cn
Full list of author information is available at the end of the article

Background

Pangolins are placental mammals belonging to the Order *Pholidota*, which contains four Asian and four African species. They are present in diverse habitats and provide ecosystem services such as natural pest control and improving soil quality. They also play an indispensable role in biological research and have implications for human health and disease studies [1, 2]. Unlike other placental mammals, pangolin skin is covered by large and overlapping keratinized scales, which provide a mechanical defense to this species (Fig. 1a-c) [3, 4]. The selective forces underlying the origin of this unique morphology remain a mystery, although they may provide a physical barrier to protect against predators. A previous study on the mechanical properties of scales from Chinese (*Manis pentadactyla*) and African (*Phataginus tricuspis*) pangolins revealed a unique structure consisting of crossed lamellae and interlocking sutures that provide

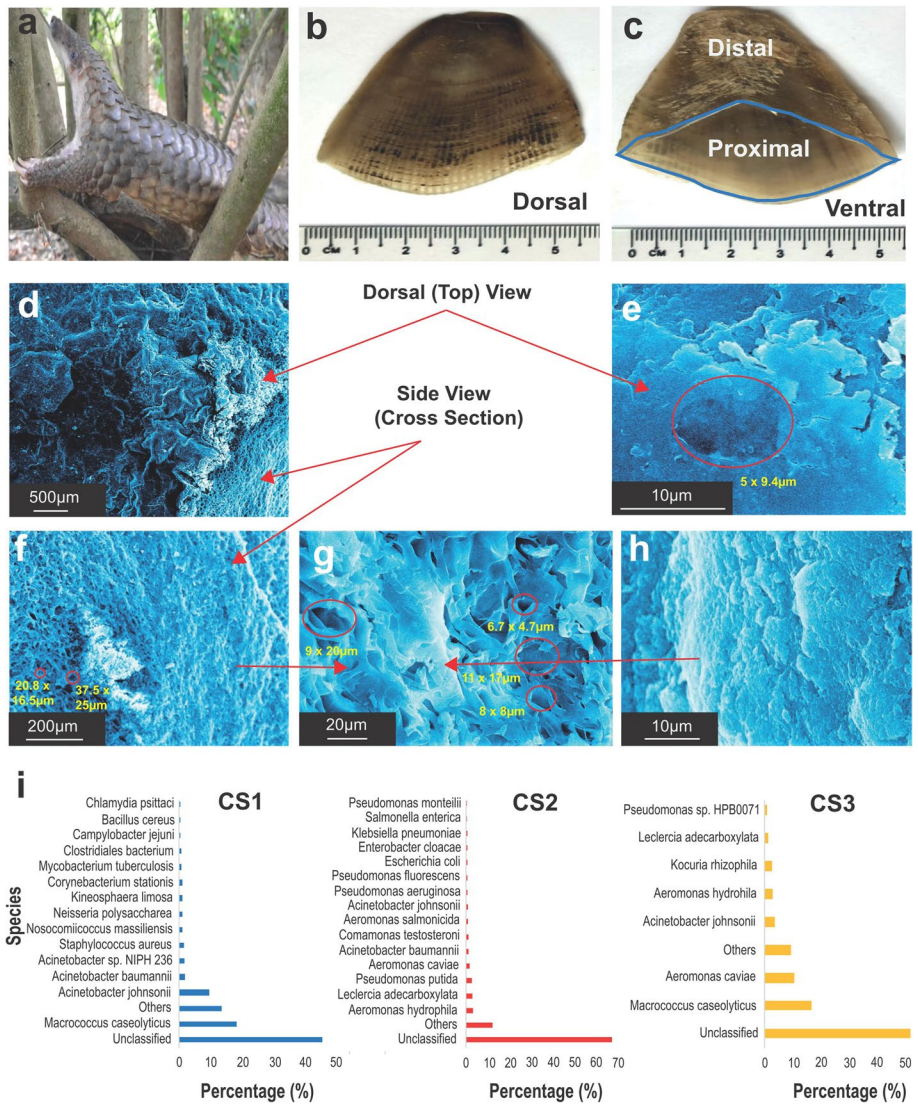

Fig. 1 Overview of scale morphology and identification of bacterial sequences. **a** A Malayan pangolin. Scales cover almost the entire body of pangolins in an overlapping manner, providing a mechanical defense for this species. **b** Dorsal view of a pangolin scale. **c** Ventral view of a scale. The dorsal surface of a scale is facing outside, whereas the ventral surface faces inside. The scale consists of two portions: the proximal portion (in the blue circle) that is attached to the skin surface, and a distal portion which is sharp, providing extra defense from predators. **d**-**h** Scanning Electron Microscopy of scales with magnifications at 30X, 85X, 900X, 1,700X and 2,200X, respectively. The dorsal (top) surface and the cross-section of the scale (side view) are shown. The pore sizes were estimated and highlighted with red circles. **i** Scale microbiome analyses of three individual pangolin scales (CS1-CS3) at the species level. We only accepted bacterial taxa with at least 0.5% abundance. Bar colors indicated the experimental sets

exceptional bonding strength and shear resistance [3]. Additional functions are suggested by their bioactivities since pangolin scales have been used in Traditional Chinese Medicine to treat ailments such as skin diseases, inflammation, rheumatic arthritis, and cancers for thousands of years. Recent work has demonstrated that pangolin scale extract exhibits anti-inflammatory activity in a rheumatic arthritis rat model [5].

We previously reported that the Interferon epsilon (*IFNE*) gene was inactivated by mutations in all pangolin species that we examined, perhaps impacting resistance to infection [6]. *IFNE* is a type I interferon, a family that exhibits antimicrobial, anti-inflammation, antitumor, and immunomodulatory activities [7]. *IFNE* is exclusively expressed in the epithelial cells of the skin and the mucosa of inner organs, contributing to the first line of defense against pathogens entering the mammalian body [8, 9]. Subsequent studies also showed the inactivation of Interferon-Induced with Helicase C domain 1 (*IFIH1*/*MDA5*), a cytoplasmic RNA sensor that helps initiate the innate immune response (i.e. induce type I interferon) to viral infection [10], and the loss of Z-DNA-binding protein (*ZBP1*) [10], cyclic GMP-AMP Synthase (*cGAS*) [11] and its interacting partner, Stimulator of Interferon Genes (*STING*) [11], Toll-Like Receptor 5 (*TLR5*), and also likely Toll-Like Receptor 11 (*TLR11)* [12] during the evolution of pangolins. Moreover, pangolins have a reduced number of the heat shock protein (HSP) gene family members, suggesting stress susceptibility that could induce immunosuppression, compared to other mammalian lineages. These observations raise an interesting evolutionary question: how have these adaptations in pangolins occurred given their seemingly increased susceptibility to infection and stress if their skin is constantly being exposed to pathogens?

Since pangolins are the only mammals that have both keratinized scales and have lost the *IFNE* gene important for skin immunity, we hypothesized that keratinized scales are an evolutionarily innovative morphology that might have evolved to compensate for decreased skin immunity (e.g., reduced pangolin vulnerability to infection and protection against injuries/stress). Here we characterized the structure, composition, and functions of scales at the molecular level in order to gain better insights into this unconventional aspect of pangolin morphology and immunity.

Results

Pangolin scales may function to trap microorganisms

To gain a better understanding of the structure of scales, we visualized scales obtained from Malayan pangolins (*Manis javanica*) using Scanning Electron Microscopy (SEM). The scale surface was generally smooth and composed of flakes stacked together to form a hard, protective layer with the particular feature of 'holes' distributed across the entire surface area (Fig. 1d-h). The side view showed a porous and honeycomb-like structure with diverse pore sizes, approximately 10-20 μm (Fig. 1g). It is possible that the presence of the pores may have no functions important for the life of pangolins. However, viruses and bacteria typically have sizes less than 10 μm and may enter into the scales through the larger surface holes and become trapped by the complexity of the intra-scale morphology [13].

To investigate whether microorganisms can enter into scales, we examined the presence of microorganisms in three individual scales (CS1-CS3) of Malayan pangolins (Additional file A: Figure S1 and Additional file B: Tables S1-2). Our data revealed the presence of microbial DNA in pangolin scales using a 16S rRNA gene amplification and also a whole-genome shotgun metagenomics approach (Fig. 1i and Additional file A: Figure S2-3) [14–18]. Metagenomics sequencing exposed that the most abundant species found within the microbiome of CS1 was *Macrococcus caseolyticus* (18.4%), followed by *Acinetobacter johnsonii* (9.6%). For CS2, the most abundant species were *Aeromonas hydrophila* (3.2%) and *Leclercia adecarboxylata* (3%), whereas *Macrococcus caseolyticus* (16.7%) and *Aeromonas caviae* (10.5%) were among the known species found within the microbiome of CS3. The scales from these three different individual pangolins showed generally different taxonomic diversity of microbiomes, probably reflecting their exposure to different environments. We also assembled genome sequences of the topmost abundant species using the metagenomics data and obtained near-complete genomes (79.9–97.9%) from these samples, suggesting the presence of microbiota in pangolin scales (Additional file A: Figure S4). Overall, the presence of microbial DNA in pangolin scales supports the view that the scale can function to trap invading microorganisms, providing the first line of defense to protect pangolins.

Scale proteome and the identification of nano-sized exosomes

To examine the protein composition of scales, we analyzed the proteomes of three individual scales (CS4-CS6) of Malayan pangolins (Additional file A: Figure S5 and Additional file B: Table S1) using high-performance liquid chromatography with tandem mass spectrometry (HPLC–MS/MS) technology. Each scale was split into two portions: a proximal portion (PS: the scale area attached to the skin) and a distal portion (DS: the scale area not attached to the skin), which yielded six experimental protein datasets in total (Fig. 1c). Sixty-one prominent proteins that fit our stringent definition of

detectability (present in at least five out of six experimental sets with protein identification probability of > 96%) were identified in the scale proteome (Additional file B: Table S3). Notably, scales are composed of flat keratinized cells that are produced when living cells die and are filled with important proteins. Therefore, it is expected that scales would not have many proteins. The majority of these proteins were predicted to be active in cellular components such as exosomes (42 genes), followed by cornified envelope (10 genes), keratin filament/desmosome (17 genes), ficolin-1-rich granule lumen/membrane (11 genes), azurophil granule lumen (4 genes), and blood microparticle (5 genes) (Additional file B: Table S4). To confirm the presence of vesicles, we isolated vesicles from pangolin scale by ultracentrifugation and visualized them using Transmission Electron Microscopy (TEM). TEM analysis revealed that exosomes in pangolin scales possessed rounded and cup-like membrane structures (Fig. 2a). Nano-flow cytometry analysis estimated these exosomes have average sizes of 73.2 ± 14.7 nm and with a concentration of 8.16×10^8 particles/mL (Fig. 2b). We conclude that pangolin scales are rich in nanoscale exosomes supported by evidence from the large number of exosome-related proteins and the exosome-like structure and size.

Pangolin scales, primarily composed of dead cells, present an intriguing source of exosomes. We hypothesized that these extracellular exosomes might originate from adjacent living cells. To elucidate their origin, we mapped 61 identified scale proteins to ExoCarta [19], an exosome database, revealing unexpected cellular sources. Substantial protein overlap was found with mesenchymal stem cells (47.5%), platelets (42.6%), thymus (34.4%), keratinocytes (27.9%), and B cells (24.6%) (Additional file B: Table S5). This diverse profile suggests contributions from stem cells, hematopoietic lineages, and epithelial cells, with the presence in blood-related sources indicating circulatory and immune system involvement.

To gain better insights into the interactome of scale proteins, we performed a network analysis using STRING [20] (Fig. 2c). The STRING functional enrichment analysis revealed three major functions: immune response (41%), response to stress (41%), and keratinization (34.4%) (Fig. 2d-f & Additional file B: Table S6).

Immune response

Immunity-related proteins were enriched in functions related to neutrophil degranulation (84%), defense response (48%), antimicrobial humoral response, and regulation of peptide transport (32%) (Fig. 2d). Interestingly, the majority of them (e.g., Lysozyme (LYZ), Secretory Leukocyte Peptidase Inhibitor (SLPI), Annexin A2 (ANXA2), S100 Calcium Binding Protein P (S100P), and Macrophage Migration Inhibitory Factor (MIF) are involved in neutrophil degranulation, the regulated exocytosis of secretory granules containing mediators such as proteases and inflammatory proteins [21]. For instance, Lysozyme (LYZ), is a well-known cornerstone of innate immunity and a critical antimicrobial protein for host defense [22]. Lysozymes have a direct antimicrobial action and work in acellular environments [22]. Another secreted protein, SLPI, is an anti-inflammatory mediator and has antimicrobial activity [23]. Two annexins, Annexin A1 (ANXA1) and Annexin A2 (ANXA2), prominent contributors to the innate immune response and anti-inflammation, were also identified [24]. Several S100 proteins (e.g., S100 calcium-binding protein A8 (S100A8) and S100 calcium-binding protein A9 (S100A9)) that are induced after infection or inflammation and exhibit antimicrobial activity were found [25]. We also identified eight proteins (e.g., Peptidylprolyl

(See figure on next page.)

Fig. 2 Characterization of exosomes, STRING interaction network and comparative analyses of 61 prominent scale proteins. **a** Analysis of exosomes in pangolin scale by TEM. **b** The size distribution profile of exosomes was analyzed by nano-flow cytometry. **c** Overview of the interactome of scale proteins revealed eight prominent clusters, representing several significant functional groupings. Cluster 1 was the largest cluster, composed of 19 proteins mainly involved in immune responses and/or responses to stress. Cluster 2 was largely composed of 14 keratin proteins. Cluster 3 was mainly composed of proteins involved in keratinisation and/or immune response. Clusters 4–6 and 8 were mainly composed of immunity-related proteins and/or those functional in responses to stress. Node colours represent the biological processes proteins are involved in. Red = keratinization; Blue = immune response; Green = response to stress. **d** Immunity response network. Red = neutrophil degranulation; Blue = antimicrobial humoral response; Green = defense response; Yellow = peptidyl-cysteine S-nitrosylation; Purple = regulation of peptide transport. **e** Stress response network. Red = defense response to other organism; Blue = secretion by cell; Purple = response to external stimulus; Yellow = response to unfolded protein; Cyan = cellular response to chemical stimulus. **f** Keratinization network. Cyan = cornification; Yellow = cell–cell adhesion; Purple = peptide cross-linking; Red = intermediate filament organization; Green = desmosome organization; Blue = cell junction assembly. Interactions between nodes are depicted by coloured lines. Different colours represent evidence from different sources such as text mining (yellow), curated database (cyan), experimentally determined (magenta), and coexpression (black). **g** Overlaps between scale and human hair proteins. Two hair protein sets from Adav et al. (2018) using the urea extraction (left) and the combined methods (right) were used for comparisons. **h** Overlaps between scale and nail proteins. **i** Overlaps between scale, hair and nail proteins

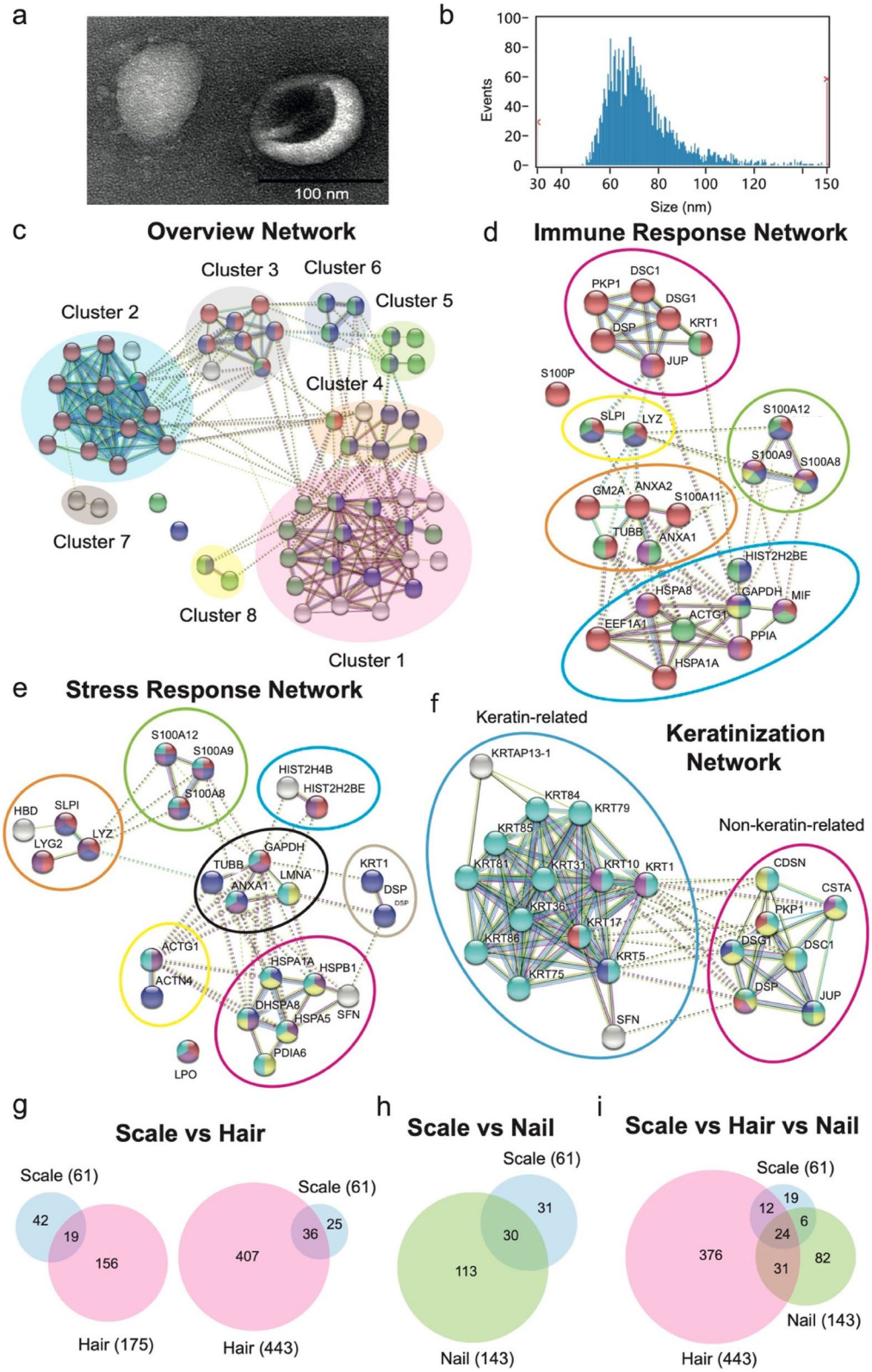

Fig. 2 (See legend on previous page.)

Isomerase A (PPIA) and Glyceraldehyde-3-Phosphate Dehydrogenase (GAPDH)) involved in the regulation of peptide transport.

Response to stress

We identified twenty-five stress-related proteins enriched in responses to external stimulus (56%), cellular response to chemical stimulus (52%), secretion by cell (48%), defense response to other organisms (36%), and response to unfolded protein (24%) (Fig. 2e). Pangolin scales may respond to external stimuli including external forces and pathogens. Nine proteins (LYG2, LPO, LYZ, SLPI, S100A12, S100A8, S100A9, HIST2H2BE, and GAPDH) are involved in protecting hosts from damage caused by other organisms. For instance, Lysozyme G2 (LYG2) works as a potent antibacterial protein, playing an important role in innate immunity [22]. Interestingly, we identified six proteins (e.g., Heat Shock Protein B1 (HSPB1), Heat Shock Protein A5 (HSPA5) and Heat Shock Protein A8 (HSPA8)) enriched in the responses to unfolded proteins, which may play a role in stress. HSPB1 is known for its antioxidant properties and functions as a chaperone to maintain proteins in a folding state, thus, it is critical in stress resistance [26].

Keratinization

Twenty-one scale proteins are involved in keratinization, an important process that forms the tough scale structure (Fig. 2f). They were divided into two distinct subclusters. One subcluster was mainly keratin proteins, likely playing an important role in the development of pangolin scales with mechanical resistance, structural stability, and water repellence. The second subcluster was composed of seven non-keratin proteins with functions such as cornification, cell adhesion, peptide crosslinking, and desmosome organization.

Together, these results suggest that pangolin scales may possess antimicrobial, anti-stress or anti-inflammation proteins that could enable defense against microorganisms and stress.

To broaden our insights, we also relaxed our protein detection criteria (present in $\geq 3/6$ experimental sets, $>96\%$ identification probability), identifying 94 proteins in the pangolin scale proteome (Additional file B: Table S7). While this approach may capture low-abundance proteins missed by stringent criteria, STRING analysis of this expanded dataset yielded similar enriched biological processes to the original 61-protein set (Additional file B: Table S8). Notably, the distribution pattern of exosome-derived cell types remained consistent with our initial findings (Additional file B: Table S9).

Comparative analysis of scale, hair, and nail

Observations of pangolins and their closest relatives (Carnivora, e.g., dogs and cats) suggest that scales might have evolved from hair. To obtain better insights into the differences between scale and hair, we compared the pangolin scale protein set with the two protein sets published for human hair: Set 1 contains 175 hair proteins using the urea extraction method, whereas Set 2 contains 443 proteins identified using three different methods [27]. Of the 61 scale proteins, 31.1% of them had orthologs among human hair proteins (Set 1) (Fig. 2g). When comparing with Set 2 of proteins, this percentage increased to 59%, whereas the remaining proteins were scale-specific. These scale-specific proteins were enriched in specific functions: response to stimulus (80%), response to stress (48%), and immune response (44%), and neutrophil degranulation (36%) (Table 1). Nearly half of them were involved in immune responses, including defense response to bacteria and fungi.

We next investigated differences in the protein composition between pangolin scales and human nails since both have been suggested to be homologous structures [28]. We compared our scale protein set with the set of 143 proteins identified in human nail [29]. Of the 61 scale proteins, nearly half were scale-specific and enriched in functions related to response to stimulus, response to stress, immune response, and neutrophil degranulation (Fig. 2h and Table 1).

By using more stringent criteria, we discarded any scale protein that can be found in human hair and nail structures, yielding 19 proteins (31.1%) that were scale-specific, which were enriched in response to stimulus (78.9%), followed by response to stress (52.6%), immune response (36.8%) and neutrophil degranulation (31.6%) (Fig. 2i and Table 1). For instance, Lactoperoxidase (LPO), a natural effective antimicrobial enzyme, contributes to host defense against infection [30] and acts synergistically with lysozyme in its antimicrobial capacity [31]. Cystatin A (CSTA) has antimicrobial activity against various bacteria and viruses, and functions in immune modulation [32]. It inhibits the growth of bacteria with its apparent bactericidal activity [33]. Hemoglobin Subunit Delta (HBD) is a component of extracellular hemoglobin that can bind to cell-derived danger-associated molecular pattern (DAMPs) agents, such as heat-shock protein and S100A8, or pathogen-associated molecular patterns (PAMPs) to alert the host innate immunity [34]. S100A8/A9 form a heterodimer called calprotectin that inhibits bacteria by sequestering transition metals [35]. Both S100A9 and S100A12 have antimicrobial activity [36]. S100A9 also acts as an effective inhibitor of replication of coronavirus [37].

Table 1 Comparative proteomic analyses. Comparisons among pangolin scale, human hair and nail proteomes. Using very stringent criteria, we removed any scale proteins that can be detected in the human hair and nail, yielding a highly confident set of 19 scale-specific proteins. These proteins were significantly enriched in immunity and stress-related processes. √=present; ×=absent. The extracellular exosome prediction was derived from the cellular component enrichment analysis performed using STRING

Gene Symbol	Gene Description	Extracellular Exosome?	Human Hair (Dataset 1)	Human Hair (Dataset 2)	Human Nail	Enriched Biological Process (STRING)
HSPA1A	Heat shock 70 kda protein 1a	Yes	×	×	×	Response to stimulus, neutrophil degranulation, immune response, response to stress
SLPI	Antileukoproteinase precursor	Yes	×	×	×	Response to stimulus, neutrophil degranulation, immune response, response to stress
S100A9	Protein s100-a9	Yes	×	×	×	Response to stimulus, neutrophil degranulation, immune response, response to stress
S100A12	Protein s100-a12		×	×	×	Response to stimulus, neutrophil degranulation, immune response, response to stress
HIST2H2BE	Histone h2b type 2-e	Yes	×	×	×	Response to stimulus, immune response, response to stress
S100P	Protein s100-p	Yes	×	×	×	Response to stimulus, neutrophil degranulation, immune response
GM2A	G(m2) activator protein	Yes	×	×	×	Response to stimulus, neutrophil degranulation, immune response
HBD	Delta-globin		×	×	×	Response to stimulus, response to stress
HIST2H4B	Histone h4	Yes	×	×	×	Response to stimulus, response to stress
PDIA6	Protein disulfide-isomerase a6 isoform b	Yes	×	×	×	Response to stimulus, response to stress
ACTN4	Alpha actinin 4	Yes	×	×	×	Response to stimulus, response to stress
LPO	Lactoperoxidase isoform 1 prepro-protein	Yes	×	×	×	Response to stimulus, response to stress
CALM3	Calmodulin-1 isoform 1		×	×	×	Response to stimulus
CALM2	Calmodulin-2 isoform 3		×	×	×	Response to stimulus
NME1	Nm23 protein	Yes	×	×	×	Response to stimulus
CSTA	Cystatin-a		×	×	×	
CDSN	Corneodesmosin		×	×	×	
SERPINA12	Serpin a12 precursor		×	×	×	
S100A2	Protein s100-a2 isoform 1		×	×	×	
KRT85	Keratin, type ii cuticular hb5 isoform 1		√	√	√	
KRT5	Keratin, type ii cytoskeletal 5		√	√	√	
KRT84	Keratin, hair, basic, 4		√	√	√	
KRT31	Keratin, hair, basic, 4		√	√	√	
KRT86	Keratin, type ii cuticular hb6		√	√	√	
KRT36	Keratin, type i cuticular ha6		√	√	√	
KRT81	Keratin, type ii cuticular hb1		√	√	√	
KRT1	Keratin 1		√	√	√	
KRTAP13-1	Krtap13-1 protein		√	√	√	
DSP	Desmoplakin isoform i/desmoplakin		√	√	√	
KRT75	Keratin, type ii cytoskeletal 75		√	√	×	
KRT10	Keratin, type i cytoskeletal 10		√	√	×	
KRT79	Keratin, type ii cytoskeletal 79		√	√	×	
SFN	14-3-3 protein sigma		√	√	×	

Table 1 (continued)

Gene Symbol	Gene Description	Extracellular Exosome?	Human Hair (Dataset 1)	Human Hair (Dataset 2)	Human Nail	Enriched Biological Process (STRING)
LYZ	Lysozyme c		√	√	×	
S100A8	Protein s100-a8 isoform a		√	√	×	
DSC1	Desmocollin-1 isoform dsc1a preproprotein		√	√	×	
KRT17	Keratin, type i cytoskeletal 17		×	√	√	
HSPB1	Heat shock protein beta-1		×	√	√	
LRRC15	Leucine-rich repeat-containing protein 15 isoform a precursor		×	√	√	
LMNA	Lamin isoform a		×	√	√	
ENO1	Alpha-enolase isoform 1		×	√	√	
PKP1	Plakophilin-1 isoform 1a		×	√	√	
GAPDH	Glyceraldehyde-3-phosphate dehydrogenase		×	√	√	
ACTG1	Actin, cytoplasmic 2		×	√	×	
TUBB	Tubulin beta chain isoform b		×	√	×	
LGALS7	Galectin-7		×	√	×	
JUP	Junction plakoglobin		×	√	×	
ANXA2	Annexin a2		×	√	×	
HSPA8	Hspa8 protein		×	√	×	
LYG2	Lysozyme g-like protein 1 precursor		×	√	×	
TXN	Thioredoxin		×	√	×	
PPIA	Ppia		×	√	×	
MIF	Macrophage migration inhibitory factor		×	√	×	
VSIG8	V-set and immunoglobulin domain-containing protein 8		√		√	
SELENBP1	Methanethiol oxidase isoform 1		√		√	
HSPA5	Hspa5 protein		×	×	√	
S100A11	Protein s100-a11		×	×	√	
EEF1A1	Elongation factor 1-alpha 1		×	×	√	
RPLP2	60s acidic ribosomal protein p2		×	×	√	
ANXA1	Annexin a1		×	×	√	
DSG1	Desmoglein 1		×	×	√	

The presence of several heat shock proteins in scales suggests that these chaperones may help pangolins to cope with stress-induced protein denaturation [38]. Our analyses reveal the pathogen defense-related proteins in the scale-specific protein set, indicating a specific role for the pangolin scale in protection from diseases compared to human nail and hair structures.

Analysis of the 19 scale-specific proteins revealed that 11 (58%) were predicted to localize in exosomes (Table 1). Extending this analysis to the larger 94 scale protein-set identified 37 scale-specific proteins, of which 22 (59%) were predicted as exosome-associated (Additional file A: Figure S6). This consistent proportion across datasets suggests a potential role for exosome-derived proteins in pangolin scales. We hypothesize that these proteins may contribute to the unique functional properties of pangolin scales, distinguishing them from other keratinized structures in humans. This finding opens new avenues for understanding the molecular basis of pangolin scale formation and function.

Identification and screening of antibacterial metabolites

We next analyzed the scale metabolome using high-throughput mass spectrometry (MS) technology. We identified 78 prominent metabolites (Additional file B: Table S10). To verify the antibacterial capability of pangolin scales, we performed a systematic pre-screening of the anti-bacterial effects of 33 metabolites identified in pangolin scale against two typical bacteria that are proved commonly present in pangolins or their

environment [39], *Escherichia coli* (Gram-negative) and *Staphylococcus aureus* (Gram-positive). We identified seven metabolites (malic acid, succinic acid, hippuric acid, fumaric acid, L-valine, citric acid, and glycine) that exhibited significant antibacterial activity (e.g., bacterial growth rates < 80% for both types of bacteria; see Additional file B: Table S11). From these, malic acid exhibited the best inhibitory effects with a Minimum Inhibitory Concentration (MIC) of 0.25C ("C" was defined as the dose of metabolites relative to their proportions in the pangolin scales) against both types of bacteria.

We next tested the antibacterial effects of a combination of malic acid and six other effective metabolites. We found that the two-metabolite combinations of malic acid can reduce MIC to 0.2C. Interestingly, the four-metabolite (malic acid, citric acid, glycine, and hippuric acid) and most higher metabolite combinations demonstrated the best inhibitory effects with a MIC of 0.1C for both *S. aureus* and *E. coli* (Fig. 3a-b and Additional file B: Table S12). Further examinations also demonstrated that the four-metabolite combination can inhibit the growth of *Pseudomonas aeruginosa* and *Serratia marcescens* (Fig. 3c-d). The antibacterial efficacy of the four metabolites was also investigated against all four bacterial species at various times of incubation. A substantial reduction was observed when the duration of the bacterial exposure to the four metabolites occurred across 24 h (Fig. 3e-f & g-h).

To understand the underlying mechanism of these metabolites, we selected the minimal combination of metabolites with the best inhibitory effect for Minimum Bactericidal Concentration (MBC) and based on their effects on bacterial cell morphology. MBC assay proved that the four-metabolite combination has bactericidal activity (MBC = ~0.4C) against *E. coli* and *S. aureus* (Additional file B: Table S13). Furthermore, SEM analyses showed there were apparent alterations in the morphology of bacterial cells after the four-metabolite treatment for 24 h. Compared with untreated bacteria, the outer membrane integrity of *E. coli* cells was damaged leaving large holes, whereas the surface of *S. aureus* cells was rough and shrunken (in some cases, the hole was formed on cell surfaces) after treatment (Fig. 3i). Altogether, our results showed that the metabolites identified in scales may kill both bacterial types by causing damage to the integrity of bacterial cells.

Metabolic and proteomic differences in pangolin scale and skin surface

We hypothesized that some active compounds may diffuse out from the scale pores and spread to the surface of pangolin skin, providing protection to the skin. To test this, we examined whether the skin surface of pangolins has metabolites similar to those found in scales. MS analysis identified 70 prominent metabolites that were collected on the skin surface by the swabbing method (Additional file B: Table S14). Of these metabolites, nearly all (98.6%) were found in scales, indicating that the two have near-identical sets of metabolites (Additional file A: Figure S7a). Metabolites were from classes such as amino acids, nucleotides, and peptides, and were enriched in pathways that are important for immunity or pathogen defense, including phenylalanine, tyrosine and tryptophan biosynthesis, arginine biosynthesis, tricarboxylic acid (TCA) cycle and purine metabolism [40–42] (Additional file A: Figure S7b). In addition, differential metabolomics analysis revealed twelve metabolites in scales that were more abundant than the metabolites on the skin surface including allantoin (80-fold increase in scales), which exhibits wound and anti-inflammatory properties, and osmolytes such as taurine (14-fold) and betaine (9.3-fold) which have been used to treat infections, inflammation or immune dysfunction in the clinical practices [43] (Additional file A: Figure S8 and Additional file B: Table S15).

To investigate whether scale and skin surfaces have similar protein profiles, we collected specimens and identified 14 prominent proteins on the skin surface using mass spectrometric (MS) technology (Additional file B: Table S16). Of these proteins, 71.4% were common on both scale and skin surfaces (Additional file A: Figure S7c). Constituent proteins were mainly enriched in cornification, defense response, inflammatory response, and response to stress. For instance, Lysozyme (LYZ), S100 calcium-binding protein A9 (A100A9), S100 calcium-binding protein A12 (S100A12), Keratin 1 (KRT1) and Actin Gamma 1 (ACTG1) were enriched in defense and stress responses against a foreign body or injury.

(See figure on next page.)

Fig. 3 Anti-bacterial activities of the 4-metabolite combination (malic acid, fumaric acid, glycine, and hippuric acid). **a**-**d** MIC assays of different concentration gradients of the 4-metabolite combination against *E. coli*, *S. aureus*, *P. aeruginosa,* and *S. marcescens* treated for 24 h, respectively. **e**–**h** Growth curves of *E. coli, S. aureus*, *P. aeruginosa*, and *S. marcescens* across different time points after treatment, respectively. (i) SEM images of *E. coli* and *S. aureus* untreated (EC = *E. coli* control; SC = *S. aureus* control) and treated (ET = *E. coli* treatment; SC = *S. aureus* treatment) for 24 h. All cells were examined using high-resolution Scanning Electron Microscopy (SEM) with magnifications at 10,000X (left panel), 30,000X (middle panel), and 60,000X (right panel), respectively. All experiments were performed using three biological replicates per group

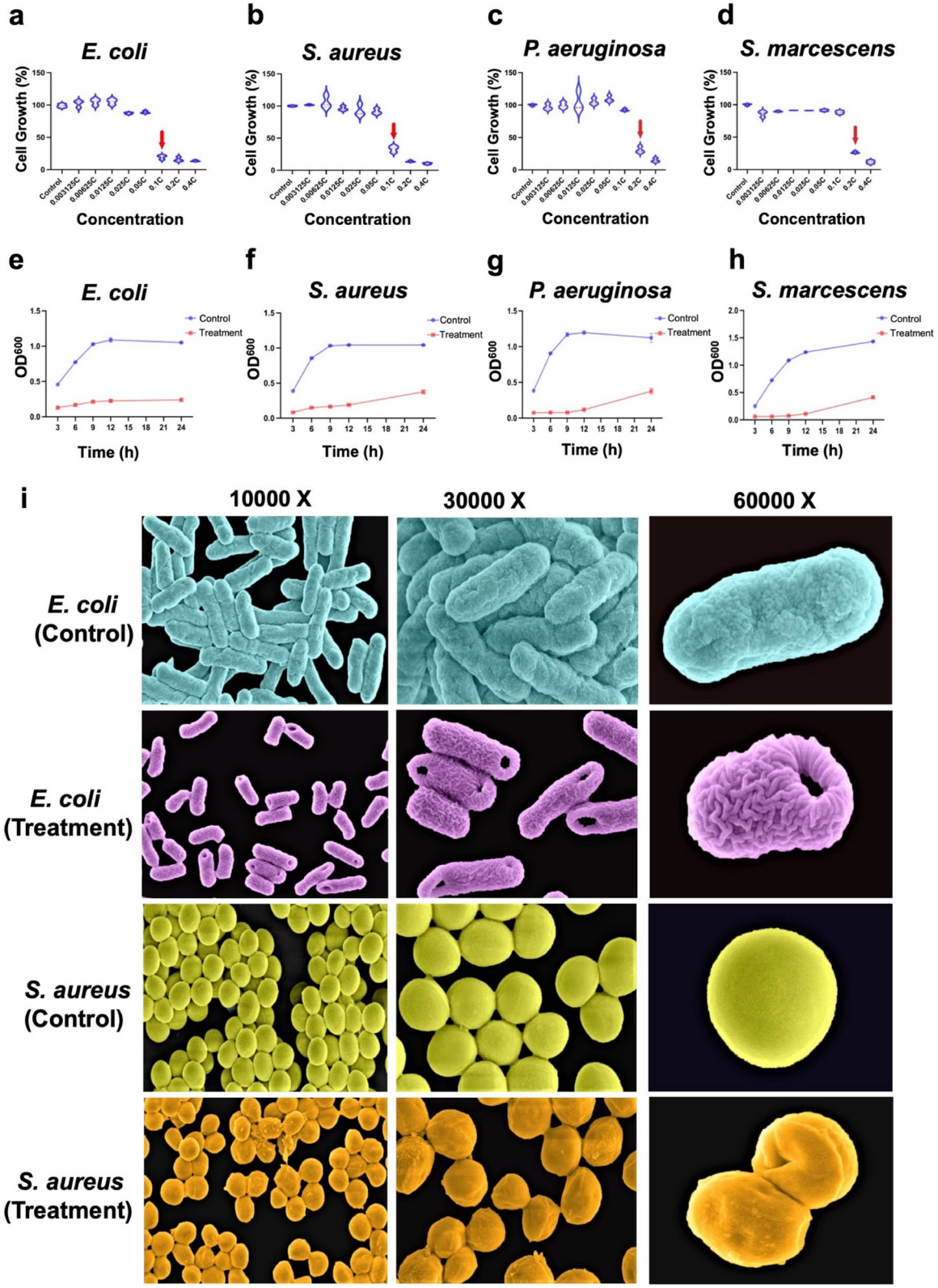

Fig. 3 (See legend on previous page.)

Moreover, A100A9, S100A12 and LYZ formed a subcluster enriched in inflammatory response to infection or injury. A100A9 is also known to contribute to wound healing, psoriasis, skin inflammation and other skin diseases field [44]. Expanding our analysis to the larger 94-protein scale set only marginally increased this overlap, resulting in 11 shared proteins (Additional file A: Figure S6). Our analyses suggest that these common proteins may help pangolins to block pathogens from invading through the skin and cope with skin stress and injury.

Discussion

Here, we report a novel functional explanation for how mammalian scales can provide host–pathogen defense. We propose a Pangolin Scale Defense Mechanism (PSDM) model to describe the functions of scales in these animals (Fig. 4). According to the PSDM, pangolin scales are large and hard, providing a strong physical barrier to protect against predators, stress and pathogens. They have a sophisticated structure and clear porous holes with diverse sizes (~ 10-20 μm in diameter). The typical sizes of viruses, bacteria, and parasites are ~ 100 nm, ~ 1 μm, and up to cm, respectively [13]. Therefore, bacteria and viruses can enter the scale through its surface pores, whereas parasites may not. Notably, the overlapping scales are large and thick, and they could be an important source for generating and storing bioactive compounds, as well as distributing them to nearly the whole skin surface in order to provide host defense against invading pathogens as well as keeping the skin healthy, including possible contributions to the prevention of skin diseases.

The evolution of pangolin scales may have been driven by multiple selective pressures such as predator protection, camouflage, a site for exchange between animal and environment, and/or for immunity (i.e., for capture of microbes). The holes within the scales could be channels for the exchange of gases or nutrients with the external environment or may help to reduce the weight of the scales. However, trapping pathogens within these pores potentially increases the risk of infection. It is possible that the secretion of antimicrobial molecules into the pores acts as a countermeasure against infection. Besides, the low water content in scales may suppress the growth of microorganisms. Ultimately, further research is needed to understand the importance of pores in pathogen defense.

Our analysis of pangolin scale proteins reveals unexpected complexity in their origin and composition, challenging the view of scales as simple, inert structures. High concordance with mesenchymal stem cell proteins (47.5%) suggests a role for multipotent progenitors in scale formation or maintenance. The significant presence of proteins associated with platelets (42.6%) and B cells (24.6%) indicates previously unrecognized involvement

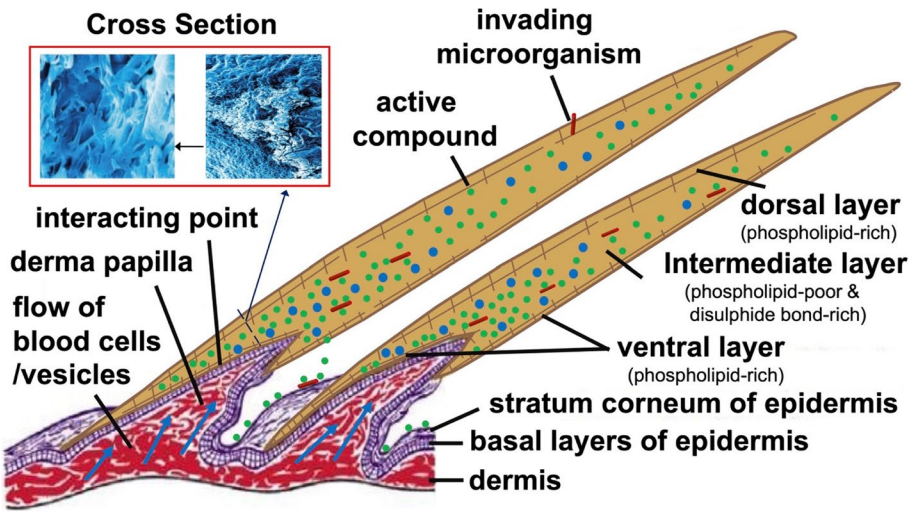

Fig. 4 Proposed Pangolin Scale Defense Mechanism (PSDM) model. Schematic diagram showing how a mammalian scale may function as a trap for microorganisms and prevent the invasion of pathogens through skin. The keratinized pangolin scale consists of three layers: (1) dorsal layer, which is rich in bound phospholipids, but is weak in disulphide bond; (2) intermediate layer, which is rich in disulphide bond, but contains no appreciable bound phospholipids; (3) ventral layer, which is only a few cells thick (interacts with the basal layers of the epidermis) and rich in phospholipids [28]. Parallel hatching represents the bound phospholipids-rich regions. Blue circles represent vesicles (e.g., exosomes), whereas green circles represent bioactive compounds (e.g., metabolites, peptides, proteins and other molecules). Red cylinder rods represent invading microorganisms. Blue arrows represent the flow of vesicles from adjacent living cells including blood cells to the interacting point/surface between scales and the basal layer of the epidermis, continuously releasing active compounds into the scale. (Modified from Gaudin et. al., 2020, *Chapter 1—Evolution and morphology", Pangolins, Biodiversity of World: Conservation from Genes to Landscapes*, Academic Press, p. 5–23)

of hematopoietic and immune-related components. We hypothesize that nanoscale exosomes from circulating blood cells could release active compounds into the scales, potentially contributing to innate immunity. This could serve as a compensatory strategy for reduced skin immunity in pangolins due to non-functional genes like *IFNE*. Furthermore, related research has revealed that hemoglobin alpha gene expression is upregulated in the outer layers of the human epidermis, suggesting that hemoglobin may play a role in resistance to oxidative stress [45]. This parallels our findings and suggests that similar mechanisms might be at play in pangolin scales. The relatively low overlap with keratinocyte proteins (27.9%) suggests unique properties distinct from typical mammalian keratin structures. These findings suggest that pangolin scale formation may involve contributions from various cell types, suggesting possible unique adaptations beyond physical protection.

Our results suggest crucial roles of scale-specific proteins in the evolution of pangolin scales and highlight specific sets of proteins found only in the scales (but not in human hair or nails), as well as pangolin scale proteins with human orthologs in hair and nails that indicate underlying commonalities. It is possible that pangolin scales evolved into more complex structures and functions in response to stimuli including stress and pathogens. Although the three keratin-based structures all originated from skin epithelial cells, they might be programmed in different ways to generate distinct morphologies with specialized functions over evolutionary time. Li et al. identified 54 differentially expressed proteins during pangolin scale development, with 17 overlapping with transcriptome changes, suggesting these proteins may play crucial roles in activating scale development [46]. None of these 17 proteins were found in our pangolin scale proteome, indicating our identified proteins likely function in mature scale structure, maintenance, or originate from exosomes of other tissues, rather than in initial development. This distinction underscores the difference between proteins involved in scale formation and those present in fully-formed scales.

Our results implicate pangolin scales as a natural storage or source of many bioactive molecules that may pass out from the ventral scale pores to the skin surface, thus protecting the skin, a possibility supported by several observations. First, the scale pores are large; therefore, smaller molecules can diffuse out from pores to reach the skin surface. Second, nearly all metabolites are common in both scales and on the skin surface of pangolins, suggesting that some of the skin metabolites may come from scales. Third, the presence of LYZ on the skin surface of pangolins could be unusual and could indicate that they might originate from scales. Fourth, pangolin scales are large and thick and cover almost the entire body, providing ideal structures to store molecules and distribute them to almost the entire skin surface. This could be an effective strategy to prevent the invasion of pathogens into the host's body and keep the skin healthy.

Due to the COVID-19 pandemic, it is difficult to collect the scales of pangolins for further analysis and validation within a reasonable timeframe. Although we have provided new insights into the potential function of pangolin scales, there is still room for improvement. For instance, it would be interesting to validate our observations using the scales of other pangolin species, which have also lost the *IFNE* gene [6]. Further examine whether scales from other vertebrate groups such as lizards, snakes, turtles, iguanas and crocodiles in these taxa have also evolved similar functions as pangolin scales. Also, some molecules not detected by proteomics and metabolomics may be important for antimicrobial action. A 'standard' approach would be to use activity-guided fractionation to identify and purify the active agent(s) in an extract like this. A key focus of future research should be to directly demonstrate that pangolin scales can trap microorganisms using fluorescence in situ hybridization, isolate potential exosomes/granules from scales for detailed analyses such as comparing the contents of these vesicles with other mammalian vesicles. Comparative quantitative proteomics of scales and other keratinized structures (e.g., hair and nails) could provide deeper insights into the unique adaptations of pangolin scale composition. Besides, bacteria from pangolin scales should be isolated to test whether they have some kind of tolerance or resistance to the antibacterial activities.

Conclusions

This study provides a new perspective on the functional significance of pangolin scales, suggesting they play an important role in host–pathogen defense. Our findings indicate that pangolin scales may trap microorganisms and generate bioactive compounds that contribute to innate immunity, potentially compensating for the reduced skin immunity in pangolins. The proposed Pangolin Scale Defense Mechanism (PSDM) model highlights the sophisticated structure and multifunctional role of scales in pathogen defense.

Our results emphasize the need for further research to explore the evolutionary adaptations of pangolin scales and their potential applications in biomimetic antimicrobial approaches. Additionally, the variability in scale microbiomes may reflect environmental exposure, offering a potential method for identifying the geographical origin of confiscated pangolin scales.

While there is limited evidence that scales provide unique benefits regarding human health, our results indicate that the active compounds identified are similar to those available commercially in purified form. We urge governments to provide more protection to these threatened species because of their high research value and ecological importance.

Methods

We present an overview of the Methods, with further methodological details provided in the supplementary methods as Additional file C [20, 47–67]. Briefly, the structure of Malayan pangolin scales was analyzed with an SEM microscope (SEM-JEOL model JSM-6510, Japan). For metagenome analysis, DNA was sequenced on the MGISEQ-2000 platform at BGI, China. The proteomes were processed and sequenced using LC–MS/MS. Network analysis of scale proteins was conducted using STRING [20]. Metabolic extracts were prepared using an extraction protocol as previously described [60]. Chromatographic separation was performed using an ultra-performance LC system (Agilent 1290 Infinity II; Agilent Technologies) and sequenced using high-resolution mass spectrometry (5600 Triple TOF Plus, Applied Biosystems/MDS Sciex, Concord, ON, Canada) equipped with an ESI source. Metabolite identification was compared with HMDB [62] and METLIN [63]. Antibacterial assays were conducted through the minimum inhibitory concentration (MIC) assay and the minimum bactericidal concentration (MBC) assay. The bacterial morphology examination was performed using SEM (Hitachi, Ltd., SU8010, Japan). Exosomes of pangolin scales were extracted by ultracentrifugation, digested with collagenase, and verified by TEM microscope (HT-700, Hitachi) and Flow NanoAnalyzer (NanoFCM INC, China).

Abbreviations

ACTG1	Actin Gamma 1
ANXA1	Annexin A1
ANXA2	Annexin A2
cGAS	Cyclic GMP-AMP Synthase
CSTA	Cystatin A
DAMPs	Damage-Associated Molecular Patterns
GAPDH	Glyceraldehyde-3-Phosphate Dehydrogenase
HBD	Hemoglobin Subunit Delta
HSP	Heat Shock Protein
HSPA5	Heat Shock Protein A5
HSPA8	Heat Shock Protein A8
HSPB1	Heat Shock Protein B1
IFIH1/MDA5	Interferon-Induced with Helicase C domain 1
IFNE	Interferon Epsilon
KRT1	Keratin 1
LPO	Lactoperoxidase
LYG2	Lysozyme G2
LYZ	Lysozyme
MBC	Minimum Bactericidal Concentration
MIC	Minimum Inhibitory Concentration
MIF	Macrophage Migration Inhibitory Factor
MS	Mass Spectrometry
PAMPs	Pathogen-Associated Molecular Patterns
PPIA	Peptidylprolyl Isomerase A
PSDM	Proposed Pangolin Scale Defense Mechanism
S100A8	S100 Calcium-Binding Protein A8
S100A9	S100 Calcium-Binding Protein A9
S100P	S100 Calcium Binding Protein P
SEM	Scanning Electron Microscopy
SLPI	Secretory Leukocyte Peptidase Inhibitor
STING	Stimulator of Interferon Genes
TCA	Tricarboxylic Acid
TEM	Transmission Electron Microscopy
TLR11	Toll-Like Receptor
TLR5	Toll-Like Receptor 5
ZBP1	Z-DNA-binding Protein

Supplementary Information

The online version contains supplementary material available at https://doi.org/10.1186/s12915-024-02034-5.

Additional file A: Figures S1-S8. Figure S1: Species identification of pangolin scales used in the metagenomic analyses. Figure S2: Bacterial 16S gene PCR amplification. Figure S3: Scale microbiome analyses at the genus level. Figure S4: Genome reconstruction and completeness of the topmost abundant bacteria species generated from whole-genome shotgun sequencing data. Figure S5: Species identification of pangolin scales used in the proteomic and metabolomic analyses. Figure S6: Comparative analysis of 94 scale protein-set. Figure S7: Metabolomic and proteomic differences. Figure S8: Comparative metabolomics analysis between scale and skin surface.

Additional file B: Tables S1-S16. Table S1: A list of sequences used in this study. Table S2: Summary stats of scale microbiomes. Table S3: List of 61 prominent proteins identified in pangolin scale. Table S4: GO term enrichment analysis of 61 scale proteins. Table S5: Distribution of 61 scale proteins across exosome-producing cells and tissues. Table S6: STRING-annotated 61 proteins identified in pangolin scale. Table S7: List of 94 prominent proteins identified in pangolin scale. Table S8: Gene Ontology Biological Process enrichment analysis of 94 scale proteins using STRING database. Table S9: Distribution of 94 scale proteins across exosome-producing cells and tissues. Table S10: List of 78 prominent metabolites identified in pangolin scale. Table S11: Screening of 33 metabolites in pangolin scales for antibacterial effects at 12 h. Table S12: Minimum inhibitory concentration (MIC) of metabolite or combination of metabolite against *E. coli* and *S. aureus*. Table S13: Minimum Bactericidal Concentration (MBC) of metabolite combination against *E. coli* and *S. aureus*. Table S14: List of 70 metabolites identified on the skin surface of pangolins. Table S15: List of 12 differentially expressed metabolites between scale and skin. Table S16: List of 14 proteins identified on the skin surface of pangolins].

Additional file C: Systemic methodologies for this study.

Additional file D: Original images from this study.

Acknowledgements

We would like to thank Professor Robert White from the University of Cambridge, and Professor Leonard Lipovich from Wenzhou-Kean University for invaluable discussions and inputs, as well as for proofreading this manuscript. This project is a part of the International Pangolin Research Consortium.

Authors' contributions

S.W.C. conceived this project. S.W.C., X.T., S.Z., and J.Z. handled sample collection. K.T.L. performed the SEM experiments. S.W.C., X.T. designed and contributed to the metagenomics, metabolomics, and TEM experiments. S.W.C., X.T., and L.C. designed primers and performed PCR experiments. X.T. and L.C. processed scale samples and extracted DNA. M.W. and J.L. generated proteomic data and performed protein identification. X.T., K.S., N.S.J., G.Y.A.T., and L.C. designed and contributed to the antibacterial assay and SEM analysis. S.W.C., K.P.K., and E.W. performed data analyses and interpretation (e.g., proteomics, metabolomics, and metagenomics data). S.W.C., X.T., Y.Y., and

L.C. contributed figures and tables. S.W.C., X.T., and L.C. wrote the manuscript, which was revised by N.S.J, K.P.K., and Y.Y. All authors read and approved the final manuscript.

Funding
This work was funded by the high-level talent recruitment programme for academic and research platform construction (Reference Number: 5000105) from Wenzhou-Kean University, the Wenzhou Municipal Key Laboratory for Applied Biomedical and the Biopharmaceutical Informatics [WB20211227000125] and Zhejiang Bioinformatics International Science and Technology Cooperation Center at Wenzhou-Kean University [WB20210429000008].

Data availability
The sequencing data in this study have been deposited in the NCBI Sequence Read Archive (SRA) under Bioproject accession number PRJNA1155658 [68]. The mass spectrometry proteomics data have been deposited to the ProteomeXchange Consortium (http://proteomecentral.proteomexchange.org) via the PRIDE partner repository [69] with dataset identifier PXD052288 [70]. The Supplementary Figures, Supplementary Tables, Supplementary Methods, and Original Data are presented as Additional file A, Additional file B, Additional file C, and Additional file D, respectively, and can be accessed online via Figshare (https://figshare.com/) at the following DOI: https://doi.org/https://doi.org/10.6084/m9.figshare.26889598 [71]. Data supporting the findings of this study are included in the published paper and additional information.

Declarations

Ethics approval and consent to participate
This work was approved (reference number: GF (2019) BASE08) by the Biology and Science Ethics Committee under the China Biodiversity Conservation and Green Development Foundation (CBCGDF).

Consent for publication
Not applicable.

Competing interests
The authors declared that there was no conflict of interest in this study.

Author details
[1]College of Science, Mathematics and Technology, Wenzhou-Kean University, 88 Daxue Road, Ouhai, Wenzhou, Zhejiang Province 325060, China. [2]Zhejiang Bioinformatics International Science and Technology Cooperation Center, Wenzhou-Kean University, Ouhai, Wenzhou, Zhejiang Province 325060, China. [3]Present Address: Zhejiang Province-Malaysia International Joint Laboratory for Modern Agriculture and Microbial Innovation, Wenzhou-Kean University, Ouhai, Wenzhou, Zhejiang Province 325060, China. [4]Present Address: Institute of Biological Sciences, Faculty of Science, Universiti Malaya, Kuala Lumpur 50603, Malaysia. [5]China Biodiversity Conservation and Green Development Foundation, Empark International Apartment, No. 69, Banding Road, Haidian District, Beijing, China. [6]Department of Biological Sciences, Xi'an Jiaotong-Liverpool University, Suzhou, China. [7]School of Dental Sciences, Faculty of Medical Sciences, Newcastle University, Framlington Place, Newcastle Upon Tyne NE2 4BW, UK. [8]Smithsonian-Mason School of Conservation, George Mason University, Front Royal, VA 22630, USA. [9]Center for Species Survival, Smithsonian's National Zoo and Conservation Biology Institute, Washington, D.C 20008, USA. [10]Dorothy and George Hennings College of Science, Mathematics and Technology, Kean University, 1000 Morris Ave, Union, NJ 07083, USA.

Received: 15 January 2024 Accepted: 4 October 2024
Published online: 14 October 2024

References

1. Choo SW, et al. Are pangolins scapegoats of the COVID-19 outbreak-CoV transmission and pathology evidence? Conserv Lett. 2020;13(6):e12754.
2. Choo SW, et al. A collective statement in support of saving pangolins. Sci Total Environ. 2022;824:153666.
3. Wang B, et al. Pangolin armor: Overlapping, structure, and mechanical properties of the keratinous scales. Acta Biomater. 2016;41:60–74.
4. Meyer W, et al. Immunohistochemical demonstration of keratins in the epidermal layers of the Malayan pangolin (Manis javanica), with remarks on the evolution of the integumental scale armour. Eur J Histochem. 2013;57(3):e27.
5. Lv H, et al. Innovated formulation of TCM pangolin scales to develop a nova therapy of rheumatoid arthritis. Biomed Pharmacother. 2020;126:109872.
6. Choo SW, et al. Pangolin genomes and the evolution of mammalian scales and immunity. Genome Res. 2016;26(10):1312–22.
7. De Andrea M, et al. The interferon system: an overview. Eur J Paediatr Neurol. 2002;6(Suppl A):A41-6; discussion A55-8.
8. Xi Y, et al. Role of novel type I interferon epsilon in viral infection and mucosal immunity. Mucosal Immunol. 2012;5(6):610–22.
9. Fung KY, et al. Interferon-epsilon protects the female reproductive tract from viral and bacterial infection. Science. 2013;339(6123):1088–92.
10. Fischer H, Tschachler E, Eckhart L. Pangolins Lack IFIH1/MDA5, a Cytoplasmic RNA Sensor That Initiates Innate Immune Defense Upon Coronavirus Infection. Front Immunol. 2020;11:939.
11. Fischer H, Tschachler E, Eckhart L. Cytosolic DNA sensing through cGAS and STING is inactivated by gene mutations in pangolins. Apoptosis. 2020;25(7–8):474–80.
12. Sharma V, et al. Convergent Losses of TLR5 Suggest Altered Extracellular Flagellin Detection in Four Mammalian Lineages. Mol Biol Evol. 2020;37(7):1847–54.
13. Parker N, Schneegurt M, Tu AHT, Lister P, Forster BM. Microbiology. Houston: OpenStax; 2019. https://openstax.org/details/books/microbiology.
14. Kimura M, Araoka H, Yoneyama A. Aeromonas caviae is the most frequent pathogen amongst cases of Aeromonas bacteremia in Japan. Scand J Infect Dis. 2013;45(4):304–9.
15. Erdem G, Long AL. Acinetobacter Species. In: Long SS, Prober CG, Fischer M, editors. Principles and practice of pediatric infectious diseases. 5th ed. Philadelphia: Elsevier; 2018. p. 851–853.e2. https://www.sciencedirect.com/book/9780323401814/principles-and-practice-of-pediatric-infectious-diseases.
16. Hansen CM, et al. Microbial Infections Are Associated with Embryo Mortality in Arctic-Nesting Geese. Appl Environ Microbiol. 2015;81(16):5583–92.
17. Gomez-Sanz E, et al. First Staphylococcal Cassette Chromosome mec Containing a mecB-Carrying Gene Complex Independent of Transposon Tn6045 in a Macrococcus caseolyticus Isolate from a Canine Infection. Antimicrob Agents Chemother. 2015;59(8):4577–83.
18. Cotting K, et al. Macrococcus canis and M. caseolyticus in dogs: occurrence, genetic diversity and antibiotic resistance. Vet Dermatol. 2017;28(6):559-e133.
19. Mathivanan S, Simpson RJ. ExoCarta: A compendium of exosomal proteins and RNA. Proteomics. 2009;9(21):4997–5000.
20. Szklarczyk D, et al. STRING v11: protein-protein association networks with increased coverage, supporting functional discovery in genome-wide experimental datasets. Nucleic Acids Res. 2019;47(D1):D607–13.
21. Lominadze G, et al. Proteomic analysis of human neutrophil granules. Mol Cell Proteomics. 2005;4(10):1503–21.
22. Ragland SA, Criss AK. From bacterial killing to immune modulation: Recent insights into the functions of lysozyme. PLoS Pathog. 2017;13(9):e1006512.
23. Hiemstra PS, et al. Antibacterial activity of antileukoprotease. Infect Immun. 1996;64(11):4520–4.
24. Zhang S, et al. Annexin A2 binds to endosomes and negatively regulates TLR4-triggered inflammatory responses via the TRAM-TRIF pathway. Sci Rep. 2015;5:15859.
25. Wang S, et al. S100A8/A9 in Inflammation. Front Immunol. 2018;9:1298.
26. Arrigo AP. Mammalian HspB1 (Hsp27) is a molecular sensor linked to the physiology and environment of the cell. Cell Stress Chaperones. 2017;22(4):517–29.
27. Adav SS, et al. Studies on the Proteome of Human Hair - Identification of Histones and Deamidated Keratins. Sci Rep. 2018;8(1):1599.
28. Spearman RIC. On the nature of the horny scales of the pangolin. Zool J Linn Soc. 1967;46(310):267.

29. Rice RH, et al. Proteomic analysis of human nail plate. J Proteome Res. 2010;9(12):6752–8.
30. Welk A, et al. Effect of lactoperoxidase on the antimicrobial effectiveness of the thiocyanate hydrogen peroxide combination in a quantitative suspension test. BMC Microbiol. 2009;9:134.
31. Gil-Montoya JA, Guardia-Lopez I, Gonzalez-Moles MA. Evaluation of the clinical efficacy of a mouthwash and oral gel containing the antimicrobial proteins lactoperoxidase, lysozyme and lactoferrin in elderly patients with dry mouth–a pilot study. Gerodontology. 2008;25(1):3–9.
32. Henskens YM, Veerman EC, Nieuw Amerongen AV. Cystatins in health and disease. Biol Chem Hoppe Seyler. 1996;377(2):71–86.
33. Agarwala KL, et al. A cysteine protease inhibitor stored in the large granules of horseshoe crab hemocytes: purification, characterization, cDNA cloning and tissue localization. J Biochem. 1996;119(1):85–94.
34. Lee SK, Ding JL. A perspective on the role of extracellular hemoglobin on the innate immune system. DNA Cell Biol. 2013;32(2):36–40.
35. Zygiel EM, Nolan EM. Transition Metal Sequestration by the Host-Defense Protein Calprotectin. Annu Rev Biochem. 2018;87:621–43.
36. Donato R. Intracellular and extracellular roles of S100 proteins. Microsc Res Tech. 2003;60(6):540–51.
37. Collins AR, Grubb A. Cystatin D, a natural salivary cysteine protease inhibitor, inhibits coronavirus replication at its physiologic concentration. Oral Microbiol Immunol. 1998;13(1):59–61.
38. Whitley D, Goldberg SP, Jordan WD. Heat shock proteins: a review of the molecular chaperones. J Vasc Surg. 1999;29(4):748–51.
39. Mohapatra RK, et al. Check list of parasites and bacteria recorded from pangolins (Manis sp.). J Parasit Dis. 2016;40(4):1109–15.
40. Jiang M, et al. Phenylalanine enhances innate immune response to clear ceftazidime-resistant Vibrio alginolyticus in Danio rerio. Fish Shellfish Immunol. 2019;84:912–9.
41. Maha IF, et al. Skin metabolome reveals immune responses in yellow drum Nibea albiflora to Cryptocaryon irritans infection. Fish Shellfish Immunol. 2019;94:661–74.
42. Badurdeen S, Mulongo M, Berkley JA. Arginine depletion increases susceptibility to serious infections in preterm newborns. Pediatr Res. 2015;77(2):290–7.
43. Haussinger D. Use of an osmolyte for treating the effects of an infection, an inflammation or an immune dysfunction. World Intellectual Property Organization; 1997. Patent No. WO/1997/038686. https://patentscope.wipo.int/search/en/detail.jsf?docId=WO1997038686.
44. Kerkhoff C, et al. Novel insights into the role of S100A8/A9 in skin biology. Exp Dermatol. 2012;21(11):822–6.
45. Tahara U, et al. Keratinocytes of the Upper Epidermis and Isthmus of Hair Follicles Express Hemoglobin mRNA and Protein. J Invest Dermatol. 2023;143(12):2346-2355.e10.
46. Li HM, et al. Combined proteomics and transcriptomics reveal the genetic basis underlying the differentiation of skin appendages and immunity in pangolin. Sci Rep. 2020;10(1):14566.
47. Jia J, et al. Molecular identification of Manis pentadactyla using DNA barcoding. Zhongguo Zhong Yao Za Zhi. 2014;39(12):2212–5.
48. Jung MK, Mun JY. Sample Preparation and Imaging of Exosomes by Transmission Electron Microscopy. J Vis Exp. 2018;131:56482.
49. Wu M, et al. One-step quantification of salivary exosomes based on combined aptamer recognition and quantum dot signal amplification. Biosens Bioelectron. 2021;171:112733.
50. Chen Y, et al. SOAPnuke: a MapReduce acceleration-supported software for integrated quality control and preprocessing of high-throughput sequencing data. Gigascience. 2018;7(1):1–6.
51. Li R, et al. SOAP2: an improved ultrafast tool for short read alignment. Bioinformatics. 2009;25(15):1966–7.
52. Peng Y, et al. IDBA-UD: a de novo assembler for single-cell and metagenomic sequencing data with highly uneven depth. Bioinformatics. 2012;28(11):1420–8.
53. Zhu W, Lomsadze A, Borodovsky M. Ab initio gene identification in metagenomic sequences. Nucleic Acids Res. 2010;38(12):e132.
54. Fu L, et al. CD-HIT: accelerated for clustering the next-generation sequencing data. Bioinformatics. 2012;28(23):3150–2.
55. Buchfink B, Xie C, Huson DH. Fast and sensitive protein alignment using DIAMOND. Nat Methods. 2015;12(1):59–60.
56. Huson DH, et al. MEGAN analysis of metagenomic data. Genome Res. 2007;17(3):377–86.
57. Langdon WB. Performance of genetic programming optimised Bowtie2 on genome comparison and analytic testing (GCAT) benchmarks. BioData Min. 2015;8(1):1.
58. Keller A, et al. Empirical statistical model to estimate the accuracy of peptide identifications made by MS/MS and database search. Anal Chem. 2002;74(20):5383–92.
59. Nesvizhskii AI, et al. A statistical model for identifying proteins by tandem mass spectrometry. Anal Chem. 2003;75(17):4646–58.
60. Yuan M, et al. A positive/negative ion-switching, targeted mass spectrometry-based metabolomics platform for bodily fluids, cells, and fresh and fixed tissue. Nat Protoc. 2012;7(5):872–81
61. Song JW, et al. Omics-Driven Systems Interrogation of Metabolic Dysregulation in COVID-19 Pathogenesis. Cell Metab. 2020;32(2):188-202 e5.
62. Wishart DS, et al. HMDB: the Human Metabolome Database. Nucleic Acids Res. 2007;35(Database issue):D521-6.
63. Smith CA, et al. METLIN: a metabolite mass spectral database. Ther Drug Monit. 2005;27(6):747–51.
64. Brodmann PD, Nicholas G, Schaltenbrand P, Ilg EC. Identifying unknown game species: experience with nucleotide sequencing of the mitochondrial cytochrome b gene and a subsequent basic local alignment search tool search. Eur Food Res Technol. 2001;212:491–6.
65. Edgar RC. MUSCLE: multiple sequence alignment with high accuracy and high throughput. Nucleic Acids Res. 2004;32(5):1792–7.
66. Kumar S, et al. MEGA X: Molecular Evolutionary Genetics Analysis across Computing Platforms. Mol Biol Evol. 2018;35(6):1547–9.
67. Garcia-Salinas S, et al. Evaluation of the Antimicrobial Activity and Cytotoxicity of Different Components of Natural Origin Present in Essential Oils. Molecules. 2018;23(6):1399.
68. Wenzhou-Kean University, Pangolin scales as adaptations for innate immunity against pathogens. CBI Sequence Read Archive (SRA). 2024. Available at: https://www.ncbi.nlm.nih.gov/sra/PRJNA1155658.
69. Perez-Riverol Y, et al. The PRIDE database resources in 2022: a hub for mass spectrometry-based proteomics evidences. Nucleic Acids Res. 2022;50(D1):D543–52.
70. Jing, L., Pangolin scales as adaptations for innate immunity against pathogens. 2024. PRIDE, https://www.ebi.ac.uk/pride/archive/projects/PXD052288.
71. Tian XC, Li; Zhou, Jinfeng; Wang, Enbo; Wang, Mu; Jakubovics, Nicholas, Pangolin scales as adaptations for innate immunity against pathogens., et al. figshare. 2024. Dataset. https://doi.org/10.6084/m9.figshare.26889598.v1.

Publisher's Note